

Chapter 20

Modal Identification Results of Quasi-statically Tested RC Frames at Different Damage Levels

Ozgun Ozcelik, I. Serkan Misir, Carmen Amaddeo, Umut Yucel, and Erkan Durmazgezer

Abstract This paper presents modal parameter identification results of two half scale reinforced concrete (RC) portal frames experimentally tested under quasi-static cyclic loading. One of the RC frames is without infill and the other one is with hollow-fired clay brick infill. The frames are progressively damaged in in-plane direction by applying increasing drifts by a displacement controlled actuator at the floor level. At each pre-determined damage states (levels), the actuator is detached from the specimen, and dynamic tests are performed. In-plane dynamic excitation used for modal identification is applied by an electro-dynamic shaker placed on the slab level. Besides, impact hammer and ambient vibration tests are also used. NExT-ERA, EFDD, and SSI-Data are the modal identification techniques used for modal parameter estimations. The purpose of the paper is multi-fold: (i) identify modal parameters of code conforming RC frames with and without infill walls at different damage levels, (ii) follow the evolution of damage level vs. associated damping ratio estimations which can potentially be used for reference-free damage level detection, and (iii) quantify the effect of broadband excitation provided by an offline shaker tuning technique on modal identification results.

Keywords Reinforced concrete frames • Infill effect • Modal parameters • System identification • Shaker tests

20.1 Introduction

Civil engineering structures are exposed to different external effects that change their dynamic characteristics. Damage can be defined as changes affecting the structural performance of a system. The fact that damage can alter stiffness, mass, and/or energy dissipation capacity of a structure, which in turn results in detectable changes in its vibration signature, is the underlying principle of vibration-based structural health monitoring (SHM) [1]. Operational modal analysis, which does not require measurement of input, is used as a technology to extract modal parameters as well as identifying damage in structures. Modal parameters to be extracted are natural frequencies, mode shapes, damping ratios. In the literature numerous surveys exist on the recent developments of structural health monitoring techniques applied to civil engineering structures based on changes in their vibration characteristics [2].

An experimental study has been carried on two one-story one-bay half scale reinforced concrete (RC) frames with and without infill wall conditions under quasi-static lateral loads. At certain drift levels, the actuator was detached from the frames and a set of low level dynamic tests were conducted; the dynamic test program includes ambient vibration, impact and various white noise (WN) tests using a shaker. Using the dynamic data associated with certain damage levels, modal parameters of the RC frames were estimated. The aims of the study are to identify the modal parameters of code conforming frames with and without infill conditions as a function of different damage levels using three different output-only system identification methods, to investigate the effect of different excitations on modal parameter estimation results including the effect of offline tuning technique in reproducing truly low root mean square (RMS) level broadband excitation, and finally to follow the evolution of damage level vs. associated estimated damping ratios that may be potentially used for reference-free damage detection.

O. Ozcelik (✉) • I.S. Misir • U. Yucel
Dokuz Eylul University, Insaat Muh. Bol, Izmir 35160, Turkey
e-mail: oozcelik4all@gmail.com

C. Amaddeo • E. Durmazgezer
Gediz University, Insaat Muh. Bol, Izmir 35665, Turkey

20.2 Test Setup and Program

20.2.1 Specimens and Test Program

Two one-story one-bay half scale reinforced concrete frames with and without infill wall conditions with a partial slab on the beam have been tested under quasi-static loads (Fig. 20.1). Columns and beam have dimensions of $150 \times 250 \text{ mm}^2$ and $150 \times 250 \text{ mm}^2$, respectively. The height and span width of the specimens are 151 cm and 250 cm, respectively. The specimens were designed by conforming the latest earthquake design code of Turkey enforcing strong column-weak beam design philosophy [3]. The concrete compressive strength used in specimens was around 50 MPa and the yield strength of the reinforcement was 420 MPa. The lateral force to the frames was applied by a displacement controlled actuator which was attached on one side to the specimen on the slab level as shown on the top right parts of Fig. 20.1a, b, and c, and on the other side a reaction wall (not shown in the figures). The actuator was connected to the slab level with an arbitrary gap between the slab and actuator head-plate so that the beam is not restraint axially by two end-plates and free to deform. 185 kN constant axial force (about 10 % of the axial load capacity of columns) was applied to each column by two hydraulic pistons to represent axial load due to upper stories.

In Fig. 20.2b, displacement pattern applied to the specimens is shown. Each drift level was repeated three times (i.e., three full cycles) in order to induce strength degradation within the same drift level. In the same figure with a circle symbol, sequence of dynamic tests is indicated. At 0 % and at the end of drift levels 0.20, 0.50, 1.0, 1.4, 2.2, and 3.5 % a set of dynamic tests were performed on the specimens in the order indicated in the figure (at the last dynamic test point when the actuator was detached there was a certain residual displacement – non-zero value). While performing the dynamic tests, the actuator was detached from the specimen to avoid any lateral stiffness contribution. Dynamic tests data is used to track the evolution of modal parameters (natural frequencies, mode shapes, and damping ratios) with respect to different damage levels for each specimen. The details of the dynamic tests are shown in Table 20.1.

Total of 142 dynamic tests have been performed on S1 and S2 including the repeatability tests. Here in Table 20.1, only the tests used for this study are shown. The data collected during all these tests were at least 8 min long. In ambient vibration tests no external excitation was applied to the specimens. In WN tests, an electro-dynamic shaker was used for external

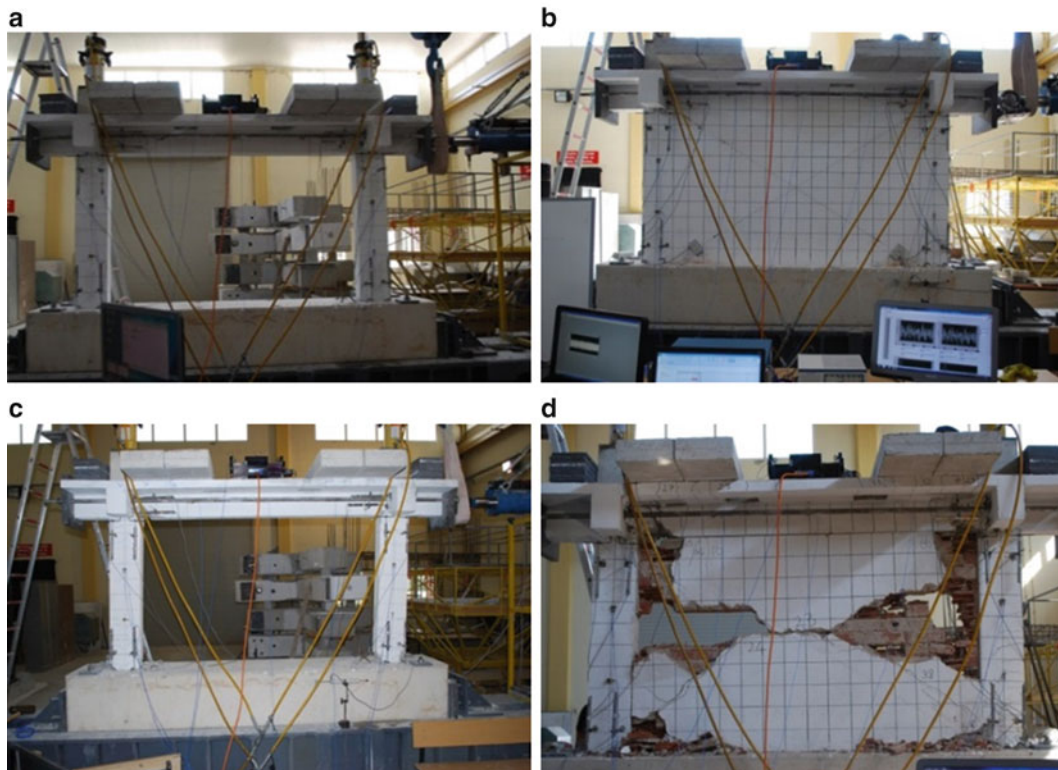


Fig. 20.1 Specimens 1 (S1 – wo/infill) and 2 (S2 – with/infill): (a)–(b) before tests; (c)–(d) after the 3.5 % drift tests

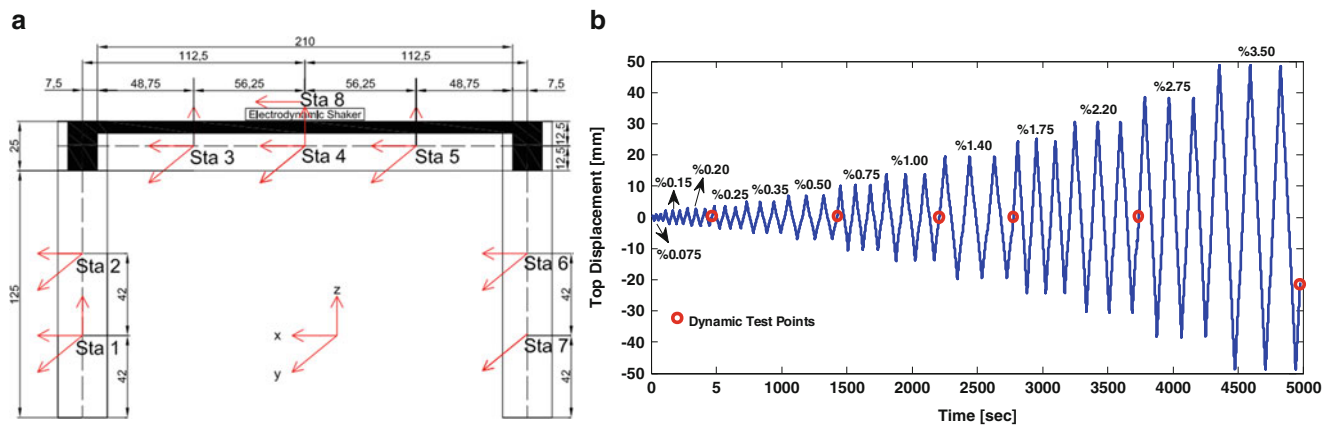


Fig. 20.2 (a) Accelerometer layout on both specimens and polarity plots of the sensors, (b) sequence of static and dynamic tests

Table 20.1 Tests performed on Specimen 1 (S1) and Specimen 2 (S2) at different damage levels

Specimen	Drift level (damage state)	Dynamic excitation type			
		Ambient	White noise (WN) wo/offline	WN w/offline-1 ^a	WN w/offline-2 ^b
S1 (S2)	No damage	NA (T3)	T31 (T1)	T32 (T6)	T32 (T6)
	0.2 %	T43 (T14)	T40 (T13)	T42 (T16)	T44 (T17)
	0.5 %	T58 (T26)	T54 (T25)	T57 (T28)	T59 (T29)
	1.0 %	T70 (T39)	T67 (T37)	T69 (T41)	T72 (T43)
	1.4 %	T85 (T56)	T82 (T55)	T84 (T59)	T86 (T60)
	2.2 %	T99 (T71)	T93 (T70)	T97 (T73)	T100 (T74)
	3.5 %	T111 (T81)	T108 (T82)	T110 (T84)	T112 (T85)

^aCommand signal to the shaker is compensated by offline tuning technique using transfer function estimate of the specimen-shaker system at the undamaged state

^bCommand signal to the shaker is compensated by offline tuning technique using transfer function estimate of the specimen-shaker system at different damaged states

excitation to the specimens, the input signal to the shaker was a clipped WN with a frequency band-width [0.5–100] Hz, the amplitude of the signal was manually adjusted using the gain knob on the signal amplifier unit, RMS value for these tests are in the order of 0.44 g, where g is the acceleration of gravity. In WN w/offline-1 and -2 tests, a control scheme called offline tuning was used to improve the signal reproduction fidelity of the shaker so that a truly broad-band excitation was achieved. Exciting the specimens with a truly broad-band signal is expected to increase the estimation accuracy. The details regarding the control scheme will be provided in the later sections, RMS values for these tests are in the order of 0.20 and 0.15 g, respectively. Note that in Table 20.1, dynamic tests performed at the end of the third cycles of each drift level were indicated.

20.2.2 Instrumentation

Both of the RC frames were instrumented with four tri-axial and six uni-axial piezoelectric type accelerometers; note that one uniaxial accelerometer was deployed on the uniaxial electro-dynamic force generator to measure the excitation (Fig. 20.2a), accelerometer stations are indicated with as “Sta”. Electro-dynamic force generator is a shaker with broadband signal reproduction capability [4]. It is used to excite the specimen under different damage states with broadband excitations. The shaker is fitted with a reaction block to increase the force level transmitted to the specimen; the shaker was placed on top of the slab (Fig. 20.2a slab level). Also, 12 displacement transducers and 2 string pots were used to measure the static response of columns, beam, and wall elements during quasi-static tests, 2 more string pots were used to measure the top displacement along the in-plane direction (x-direction). Static measurements were done using a static data acquisition system whereas for dynamic measurements a separate 18 channel 24-bit dynamic data acquisition system was used. Here only dynamic test results are presented.

20.3 Damages Observed During Quasi-static Tests

Very thorough damage observations have been done for each specimen by means of visual observation and photos. Due to page limitations, here in Tables 20.2 and 20.3, only a brief description of the observed damages at certain drift ranges are given for S1 and S2, respectively. Very concise damage observations had to be given here, and while doing this, prominent features of the observed damages are kept so that modal parameter changes can be associated with these damages.

From damage observation given in these tables, it can be seen that both specimens gradually went through substantial amount of damage. One of the main purposes of this presented study is to associate these damages with the changes observed in the modal parameters estimated using output-only system identification methods. It can also be seen that infill wall has contributed substantially to the maximum lateral strength of the frames. It should be noted here that no out-of-plane deformation was observed throughout the tests.

20.4 Offline Tuning Technique to Increase Signal Fidelity

For modal parameter estimations using output-only methods, it is important that the system to be identified is excited by broadband excitation. In this study, an electro-dynamic force generator capable of broadband excitation was used. But a close look at the signal reproduction fidelity of the shaker shows that although the input signal is broadband, the reproduced

Table 20.2 Damage observations for S1 (wo/infill) at different damage levels (at the end of each drift range, dynamic tests were performed)

Drift range [%]	P_{\max} range [kN]	Major features of the observed damages
0.075–0.2	28.3–56	No visible damage observed until the end 0.15 % drift. Within 0.2 % drift flexural hairline cracks observed at column (bottom ends) and beam ends
0.25–0.5	67–91	More tensile cracks (flexural) observed at beam and column ends (bottom ends), some hairline cracks observed at beam-column joint panel, some beam cracks extended to the slab
0.75–1.0	105–114	New flexural cracks observed along both columns, some hairline cracks emerged at beam-column joint panel, already existing flexural cracks on the columns are in the range of 2 mm, new flexural cracks observed at the slab midspan
1.4	119	Existing cracks propagated and extended on both columns and beam, new flexural cracks observed on the beam and slab, at some points on the columns concrete cover started falling off
1.75–2.2	122–109	Concrete crushing observed at column ends, some early cracks observed on the beam ends progressed to about 1 cm, plastic hinge mechanisms were visible at beam ends, concrete spalling observed at beam and column ends, uplift between foundation and right column observed, at the end of this drift range, stirrups at beam ends were visible. Maximum lateral strength of 122 kN was reached within 1.75 % drift
2.75–3.5	114–100	Significant amount of concrete crushing observed at column bottom ends, column cover concrete spalled off, buckling of beam longitudinal reinforcements on both ends and eventually rupturing occurred, long. reinforcements were clearly visible and the cracks were in the order of 1.5 cm

Table 20.3 Damage observations for S2 (w/infill) at different damage levels (at the end of each drift range, dynamic tests were performed)

Drift range [%]	P_{\max} range [kN]	Major features of the observed damages
0.075–0.2	94–168	No visible damage observed until the end 0.15 % drift. Within 0.2 % drift masonry panel separated from the frame borders
0.25–0.5	184–250	First horizontal tension cracks (hairline) observed at column bottom ends
0.75–1.0	255–237	First diagonal cracks observed within the wall, existing flexural cracks propagated at both column ends, new flexural cracks on the columns emerged, horizontal cracks formed on the central zone of the wall, wall plaster started to spall-off. Maximum lateral strength of 255 kN was reached within 1.0 % drift level
1.4	213	Existing column cracks close to the mid-height propagated, significant wall plaster spalling observed, new flexural cracks appeared on the columns, diagonal cracks on the wall extended significantly and new horizontal panel cracks observed. Flexural cracks on beam ends observed. Uplift between column ends and foundation was visible
1.75–2.2	188–162	Excessive infill wall damage observed (some wall units fell off), plastic hinge mechanism developed on the beam ends, some beam bottom tension reinforcements were visible, and buckling of long. reinforcement at beam ends were slightly visible
2.75–3.5	140–120	Cover concrete on beam ends spalled off and the long. reinforcements were clearly visible, first buckling occurred, later some bottom tension reinforcements ruptured, crushing of concrete at column bottom ends were observed, long. reinforcement on column ends were visible

feedback signal is far from being broadband. Figure 20.3a shows the transfer function estimate of the shaker when the shaker was placed on different surfaces, namely: (i) on a firm ground, (ii) on the specimen's slab when the specimen (S1) was at undamaged state, and (iii) on the specimen (S1) when the specimen was damaged at 3.5 % drift level (similar results were obtained for S2 but not shown here for the sake of conciseness). It should be noted here that for the last two cases, there is specimen-shaker interaction. All three transfer functions are very similar to each other showing that there is almost negligible specimen-shaker interaction taking place at the excitation levels used for this study. On the other hand, the transfer function estimations clearly show that the shaker will not be able to reproduce the input signal (broadband nature) both in terms of amplitude and frequency content. Figure 20.3b clearly shows this problem; here “input” is the desired signal and “output” is the measured acceleration of the shaker platform by an accelerometer mounted there (Sta 8). In order to remedy this problem in a fast and efficient way, offline tuning technique is used. In this technique, the input signal (desired signal) is multiplied by the inverse of the estimated transfer function in the frequency domain, and then transferred back to time domain using the discrete time inverse Fourier transform. This modified input signal is used as the new input to the shaker. The result of this technique in signal reproduction fidelity is shown in Fig. 20.3c – zoomed to certain portions. It is very clear that this time the desired input and output signals (signal reproduced on the platform of the shaker) match both in time and frequency domains. Moreover, the output signal has the desired broadband nature. Transfer functions used for offline tuning can be various as noted above; but also at each damage state of the specimens a new transfer function can be estimated and used for tuning purposes. In order to investigate the effects of damage states on transfer functions estimations a systematic study was carried out. Tests shown in Table 20.1 indicated as “WN Tests w/offline-2” were performed to investigate this effect. In these tests, new transfer functions corresponding to the indicated drift levels were estimated and used for offline tuning; in other words transfer functions were adapted to the new conditions of the specimens. In “WN Tests w/offline-1” tests only a single transfer

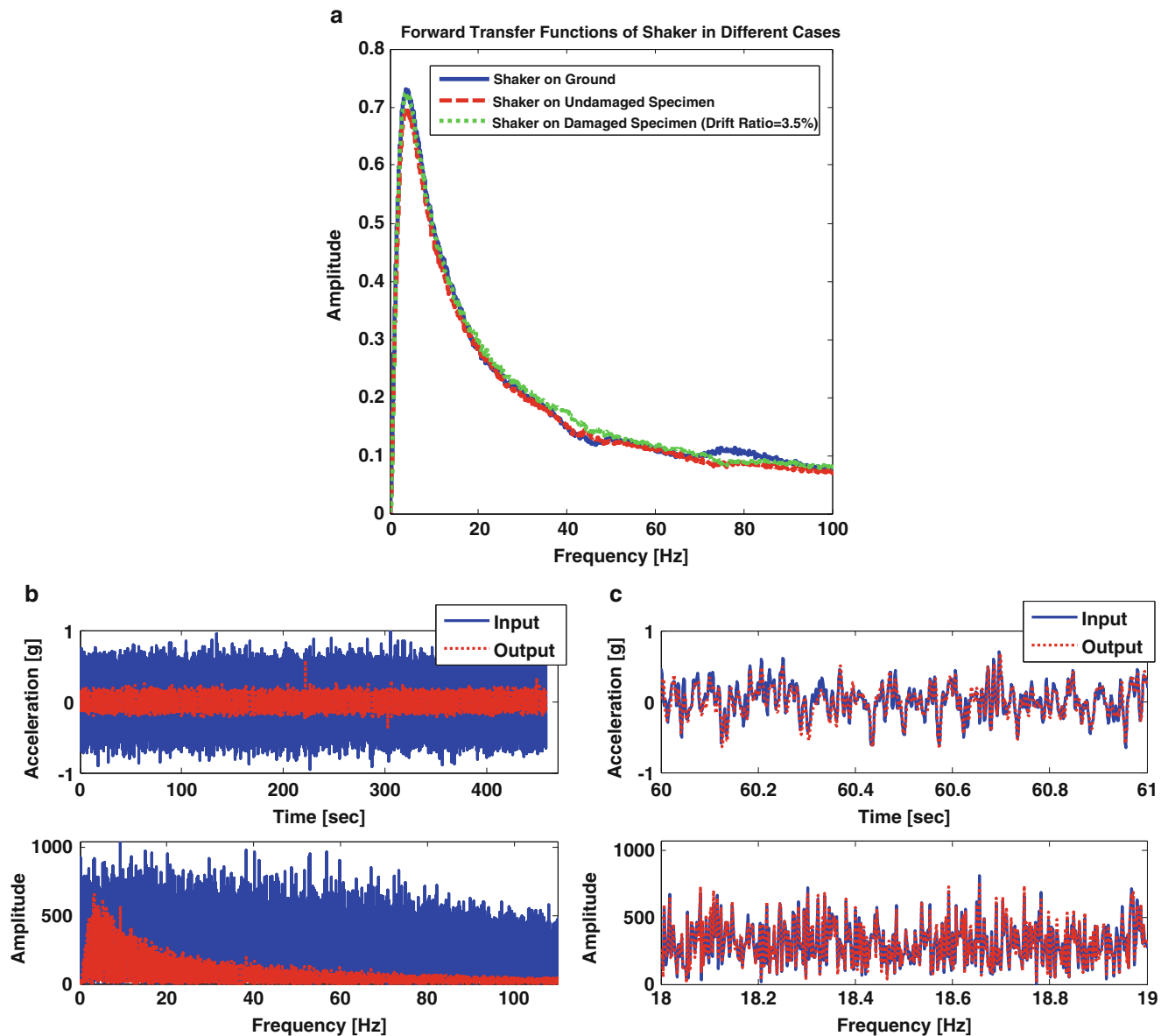


Fig. 20.3 (a) Forward transfer function estimations, (b) signal reproduction fidelity before offline tuning, (c) signal reproduction fidelity after offline tuning (zoomed)

function was used, which is the transfer function corresponding to the undamaged specimen condition. Signal reproduction fidelity is expected to affect modal parameter estimations. The modal parameter estimation results will be presented later in the paper.

20.5 System Identification Methods Used for Modal Parameter Estimation

Three different output-only system identification methods were used to estimate the modal parameters of specimens at different damage levels. These methods are (i) Data-driven Stochastic Subspace Identification (SSI-Data), (ii) Natural Excitation Technique with Eigensystem Realization Algorithm (NExT-ERA), and (iii) Enhanced Frequency Domain Decomposition (EFDD). Also, for impact hammer tests, ERA method was used, but these results are not included herein. In the paragraphs below, brief descriptions of the methods are presented.

20.5.1 SSI-Data

The SSI-DATA method obtains the mathematical model in linear state-space form based on the output-only measurements directly [5]. One of the main advantage of the method compared to two-stage time-domain system identification methods such as covariance-driven SSI and NExT-ERA, is that it does not require any pre-processing of the data to calculate auto/cross correlation functions or spectra of output measurements. One other advantage of the method is that QR factorization, singular value decomposition (SVD) and least squares are involved as robust numerical techniques in the identification process. Modal parameters such as natural frequencies, damping ratios, and mode shapes of the dynamic system can be identified. SSI-Data method is not programmed within the presented study, instead commercial ARTEMIS[®] operational modal analysis software is used where the method, among other system identification methods, is available. SSI-Data results obtained will serve as reference values to be compared with the results obtained using other two methods.

20.5.2 NExT-ERA

The underlying principle of NExT method is that cross-correlation function calculated between two response measurements (output) from a structure excited by broadband excitation has the same analytical form as the free vibration or impulse response of the structure. Therefore modal parameters can be estimated using cross-correlation functions [6]. One of the main advantages of NExT method is the ability to identify closely-spaced modes and corresponding modal parameters [6, 7]. Once the auto- and/or cross-power spectral density functions are estimated, correlation functions in time-domain are obtained by discrete inverse Fourier transform. These functions can either be used directly or be used at the next stage with ERA method to estimate modal parameters. There are numerous techniques used for identifying modal parameters from free vibration/impulse response data [2]. Here ERA method is used to extract modal parameters and model reduction of linear systems. The method is first proposed by Juang and Pappa (1985) to identify modal parameters of multi-degree-of-freedom system using free vibration response [8]. In ERA method, Hankel matrix is formed using free vibration response of the system. By applying singular value decomposition (SVD) to the Hankel matrix, the rank (i.e., model order) can be determined in the case of noise free measurement. Since real life measurements are always noisy, the model order can be determined by sorting the singular values in descending order, and performing partitioning of the SVD decomposition accordingly. Smaller singular values correspond to computational (nonphysical) modes whereas larger singular values correspond to the real physical modes. Once the model order is determined, based on the realization algorithm, the estimates of discrete-time state space matrices can be constructed. From the reduced order state space realization and sampling interval natural frequencies, damping ratios, and mode shapes can be obtained. In this study, NExT-ERA method is programmed in Matlab[®] programming environment.

20.5.3 EFDD

As an output-only method the Frequency Domain Decomposition (EFDD) method is an extension of classical pick picking (PP) technique and is based on the classical frequency domain approach also known as basic frequency domain technique. The classical technique has shortcomings such as identifying closely-spaced modes and furthermore frequency estimates are limited by the frequency resolution of power spectral density estimates and damping estimations are highly uncertain [9]. In EFDD method, *output* power spectral density (PSD) matrix is estimated at discrete frequencies then the spectral matrix is decomposed using SVD. The corresponding mode shapes can be extracted from the singular vectors. In EFDD, natural frequencies and damping ratios are estimated using PSD functions of single-degree-of-freedom systems by transforming them back to time domain using inverse discrete Fourier transform. Auto-correlation function for a SDOF system in time domain can be used for estimating frequency and damping values by using zero-crossing times and logarithmic decrement. EFDD method is programmed in Matlab[®] programming environment.

20.6 Modal Parameter Estimation Results

Modal parameter estimations for specimens S1 and S2 under different excitation conditions are given in Tables 20.4 and 20.5, respectively. WN w/offline-1 and WN w/offline-2 results are described above, the same description holds also for the following tables. Impact hammer test results were processed with ERA; but will be presented in another study. Results given in the tables are obtained with SSI-Data method. Results obtained using the other two methods could not be presented due to space limitation; but a general comparison will be presented later using bar plots. It should be noted that for S1, ambient vibration tests for the undamaged case is missing, therefore the results for these tests are indicated as “NA” in Table 20.4. In Table 20.5 for S2 (w/infill), for certain damage cases (undamaged, 1.0 % and 1.4 %) from ambient vibration tests no modal parameters could be extracted (indicated with the symbol “-”).

From the results it can be observed that different excitation conditions resulted in similar values. One important result is that the smallest natural frequency estimates are obtained from the WN wo/ offline tests. This is due to the fact that, although slightly larger, RMS values for these tests are larger than the other three tests. From this perspective, also note that the highest frequency estimates are obtained from the AV tests. MAC values given in the tables are calculated between the modes corresponding to the *undamaged state* (using the test WN w/Offline-1 test – reference case and SSI-Data method) and the modes for the damaged cases (using all other tests and SSI-Data estimations). It can be observed that as the damage level increases the MAC values between the undamaged and damaged cases decreases. Notice that at 2.20 % drift, there is a dramatic decrease in the MAC value. Although not shown here, NEXt-ERA method was able to estimate modal parameters under AV data better than SSI-Data and EFDD methods, meaning that modal parameters could be extracted successfully at all damage states even under very low level ambient vibrations.

Table 20.4 Modal parameter estimation results for S1 (wo/infill) under different excitation conditions using SSI-Data system identification method

Excitation type	Modal params	No damage	0.2 %	0.5 %	1.0 %	1.40 %	2.20 %	3.50 %
Ambient vibration	ω [Hz]	NA	14.17	13.33	12.28	11.81	10.55	9.03
	ξ [%]	NA	1.709	0.809	1.032	0.635	0.587	0.310
	MAC	NA	0.987	0.979	0.964	0.960	0.944	0.920
WN wo/offline	ω [Hz]	14.14	13.61	12.76	11.7	11.26	9.99	8.41
	ξ [%]	1.017	1.518	1.606	1.505	1.725	1.305	2.082
	MAC	0.997	0.986	0.931	0.951	0.944	0.943	0.910
WN w/offline-1	ω [Hz]	14.28	13.79	12.99	12.01	11.53	10.28	8.68
	ξ [%]	1.515	1.194	1.697	1.626	1.036	1.083	1.387
	MAC	1	0.987	0.917	0.958	0.959	0.945	0.917
WN w/offline-2	ω [Hz]	14.28	13.79	13.01	12.08	11.60	10.40	8.78
	ξ [%]	1.515	1.246	2.137	1.586	0.884	1.101	1.174
	MAC	1	0.987	0.953	0.964	0.960	0.946	0.918

Table 20.5 Modal parameter estimation results for S2 (w/infill) under different excitation conditions using SSI-Data system identification method

Excitation type	Modal params	No damage	0.2 %	0.5 %	1.0 %	1.40 %	2.20 %	3.50 %
Ambient vibration (AV)	ω [Hz]	–	17.97	18.13	–	–	16.51	11.82
	ξ [%]	–	3.947	1.998	–	–	1.992	1.442
	MAC	–	0.903	0.974	–	–	0.445	0.977
WN wo/offline	ω [Hz]	18.02	17.49	17.89	17.67	16.7	16.01	10.87
	ξ [%]	1.59	3.212	2.315	3.538	4.24	3.004	2.448
	MAC	0.999	0.983	0.980	0.938	0.966	0.607	0.795
WN w/offline-1	ω [Hz]	18.08	17.74	17.60	17.48	16.94	16.11	11.63
	ξ [%]	1.544	1.964	2.867	2.69	2.378	1.284	2.059
	MAC	1	0.986	0.913	0.898	0.951	0.817	0.820
WN w/offline-2	ω [Hz]	18.08	17.68	17.66	17.48	17.08	16.17	11.80
	ξ [%]	1.544	1.436	2.804	2.889	2.182	1.411	1.89
	MAC	1	0.988	0.898	0.966	0.903	0.835	0.811

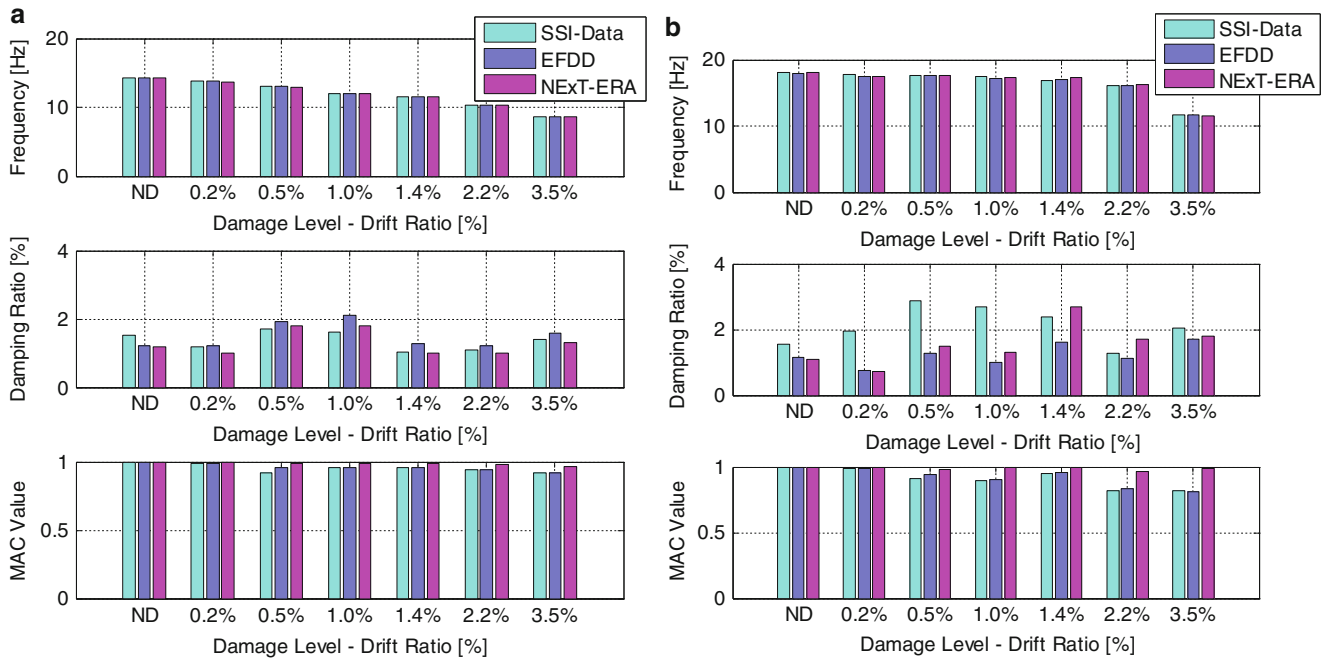


Fig. 20.4 Modal parameters evolution of (a) S1 and (b) S2 specimens estimated with SSI-Data for different damage levels under WN excitation with offline tuning using transfer function estimated for undamaged state

Figure 20.4a and b show the modal parameter estimations for S1 and S2 using different system identification methods but using only the WN w/offline-1 tests, respectively. For the natural frequency and MAC estimations, all methods give very similar results. It is clear that frequency values decrease as the damage level increases as expected. MAC values are calculated between the undamaged mode (estimated using WN w/offline-1 tests and SSI-Data method) and damaged modes (estimated using WN w/offline-1 tests and other methods). Largest variations in the results among the methods, especially for S2, are observed in damping estimations. Damping estimations by SSI-Data for S2 specimen are consistently larger than the estimations with other methods, namely NEXT-ERA and EFDD.

Figure 20.5a shows a closer look at the changes observed in natural frequency and damping estimations for S1 and S2 as a function of damage levels. Undamaged longitudinal in-plane natural frequencies for S1 and S2 are estimated to be 14.28 and 18.08 Hz, respectively. Inclusion of infill wall increases the natural frequency about 27 %. From the frequency plots, it is very clear that there is a steady decrease in natural frequencies as the damage level increases both for S1 and S2. S1 (wo/infill) loses its lateral stiffness faster than S2 specimen (w/infill), this is somewhat an expected condition since, although gets damaged, the infill wall contributes substantially to the lateral stiffness of the frame. At the ultimate damage states at 3.5 % drift level, estimated natural frequencies for S1 and S2 are 8.68 and 11.63 Hz, respectively. Therefore the changes are 39 % and 36 %, respectively. The total change in natural frequency for S2 is slightly lower than S1. This result is somewhat counterintuitive since the frame-infill interaction was expected to be more prominent for S2 even at this damage level. If the curve for S2 is investigated more closely, it can be seen that the curve has a very small negative slope up to 2.2 % drift (a higher wall contribution up to this level), and a sharp drop right after that at 3.5 % (wall contribution suddenly drops). The plot for the damping ratio estimations shows that estimated ratios for S2 are larger than S1. This observation indicates that infill wall contributes to the damping level in RC frames. It is interesting to note that a similar trend is observed for S1 and S2 specimens, except that the values for S2 are shifted upwards. Again for 2.2 % drift level, there is a sudden drop in the estimated damping value. This observation may be a supporting evidence for the fact that at 2.2 % drift infill wall contribution falls down substantially.

In Fig. 20.5b damping value estimations for S1 and S2 are given under low and high level WN excitations. Here the low level excitations are WN w/offline-1 tests, and the high level excitations are WN wo/offline tests. It should be noted that although for the high level excitations the amplitude was higher (RMS level 0.44 g) it was not substantially higher than the low level excitations (RMS level 0.20 g) due to shaker’s stroke limitations. It is interesting to note that for S1 (wo/infill), damping estimations are less sensitive to the excitation amplitude levels whereas for S2 (w/infill wall), damping estimations are more sensitive to the excitation amplitude. Again for the high level excitations there is not a clear trend in damping estimations as damage level increases.

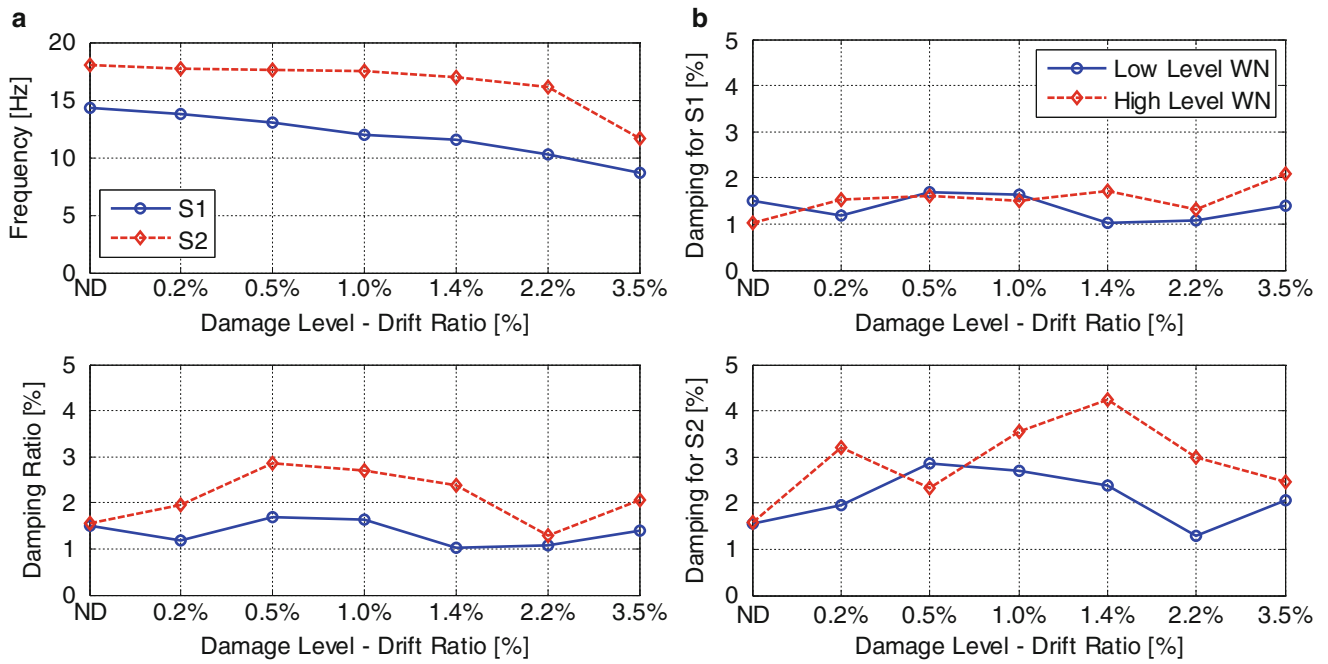


Fig. 20.5 (a) Change in frequency and damping estimations with increasing damage levels for S1 and S2 specimens, (b) effect of excitation level on damping estimations for S1 and S2 specimens

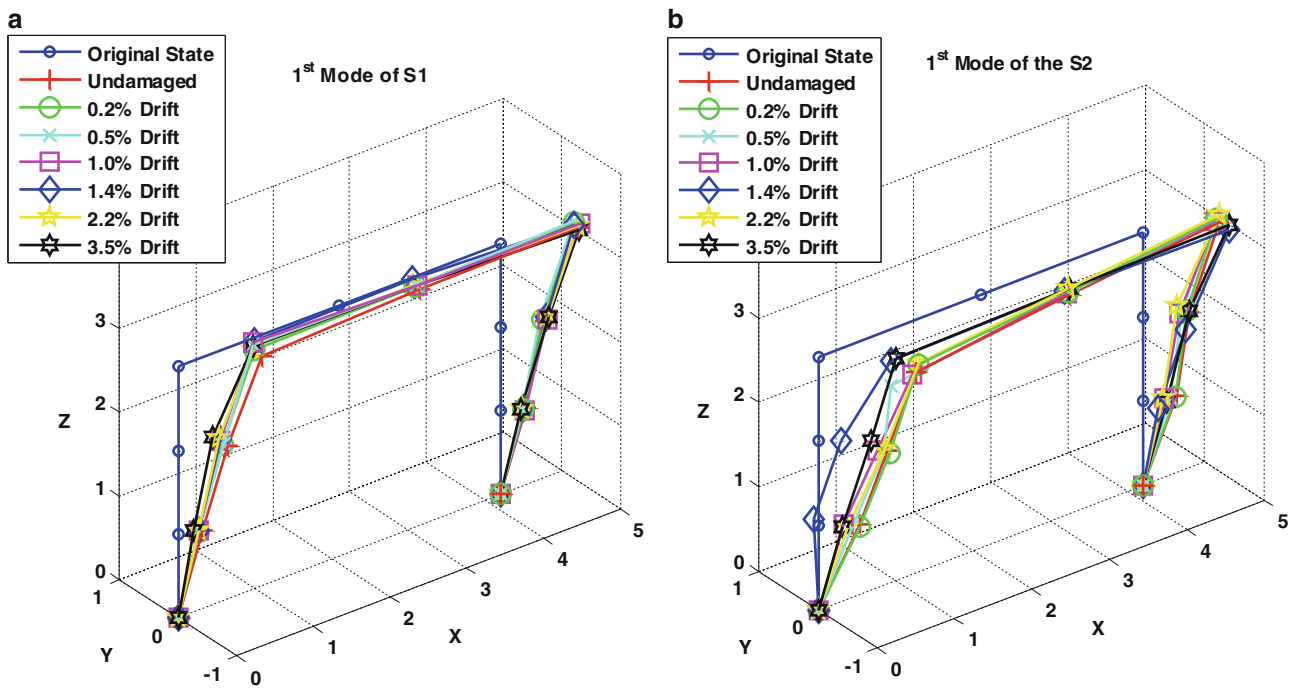


Fig. 20.6 Mode shape estimations at different damage levels using NEXt-ERA method under WN w/offline-1 tests (offline tuning exists), (a) S1 and (b) S2

Figure 20.6a and b shows the longitudinal in-plane mode shape estimations for S1 and S2 using by NEXt-ERA method using WN w/offline-1 data, respectively. It can be seen from the figures that mode shapes change as damage level changes. It is important to note that in S2 (w/infill) mode shapes seem a bit more sensitive to the damage level (notice the dramatic change at the end of drift level 1.4 %). It should also be noted that these modes are called in-plane lateral mode due to the

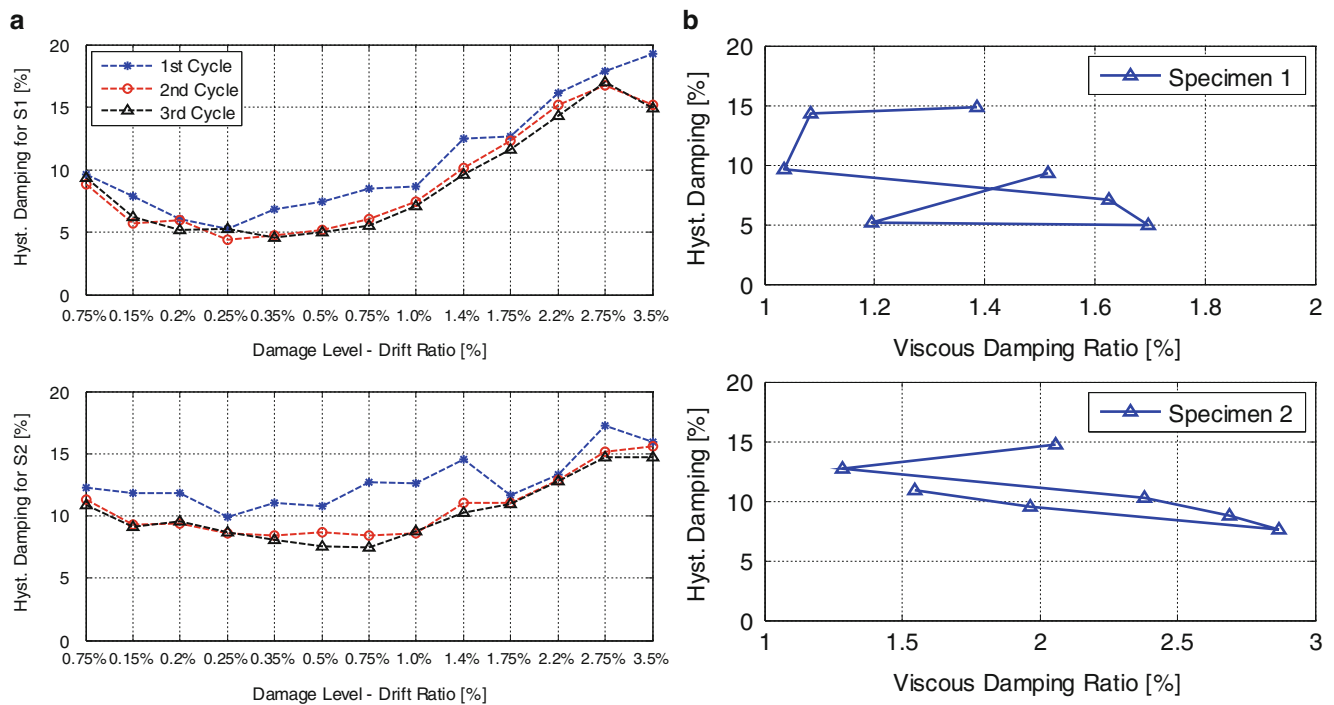


Fig. 20.7 (a) Hysteretic damping values vs. different damage level, (b) hysteretic damping vs. estimated modal damping values for S1 and S2

fact that main motion is along x-direction, but they have also components along y- and z-directions. In other words, there is no purely in-plane lateral mode but all the estimated modes (also the ones not shown here for space limitations) are coupled modes.

20.6.1 Hysteretic Damping

It is known that there is not a direct/strong relation between equivalent viscous damping and hysteretic damping (a function of the area under the hysteretic force-displacement curves) [10]. However, it would be insightful to show the change of hysteretic damping vs. estimated viscous damping coefficients as a function of damage levels. Figure 20.7a shows a plot of the calculated hysteretic damping ratios for S1 and S2 for each cycle for all drift levels, and Fig. 20.7b shows plots of hysteretic damping at the third cycle of some drift levels vs. estimated damping ratios for S1 and S2 using WN w/offline-1 tests by the SSI-Data method at that corresponding drift level. It is clear that there is not a clear trend between hysteretic damping and viscous damping estimations at this excitation levels; but at much higher excitation levels, which is not possible to induce with the available shaker in hand, a relation between these two damping values may exist.

20.7 Conclusions

In this study two half-scale reinforced concrete frame system with and without infill conditions were tested quasi-statically under increasing lateral drifts. At certain drift levels, dynamic tests were performed and modal parameters at different damage levels are estimated using three different output-only system identification methods, namely SSI-Data, NExT-ERA, and EFDD. Dynamic excitation was applied to the specimens from the slab level by an electro-dynamic shaker; also effects of offline-tuning technique is investigated which is a practical control technique to improve the signal reproduction fidelity of the shaker therefore providing a truly broad-band excitation. Main outcomes of the presented study are as follows: (i) although small, different excitations lead to different modal parameter estimations, specifically AV tests result in higher natural frequency estimates than WN w/offline, WN w/offline-1, WN w/offline-2 tests, (ii) SSI-Data, NExT-ERA and

EFDD methods give very similar modal parameter estimation results under different excitation conditions, NExT-ERA gives the best results in AV tests -under very low level excitation as compared to the other two methods, (iii) infill wall increased the lateral stiffness of the frame substantially leading to 27 % increase for the frequency of the longitudinal in-plane lateral mode, (iv) at the end of ultimate drift level of 3.5 % decrease observed in the natural frequencies for S1 and S2 are 39 % and 36 %, respectively, (v) decreasing trend in the natural frequency as a function of damage for S2 is slower than S1, (vi) it is observed that the contribution of the wall to the lateral stiffness of the frame goes down substantially at 2.2 % drift, (vii) infill wall contributes also to the damping levels of RC frames, (viii) excitation level affects the damping estimations, meaning that higher excitation levels lead to higher damping values especially when infill wall exists, (ix) at the excitation levels considered, there is not a clear relation between hysteretic and estimated viscous damping values; therefore more has to be done to associate damage with damping values estimated with the methods studied here.

Acknowledgment Authors greatly acknowledge the financial support provided by The Scientific and Technological Council of Turkey (TUBITAK) under the grant no. 112 M203. Authors also would like to thank undergraduate students Muhammed Demirkiran, Filiz Vargun, Gokhan Okudan, Mazlum Yagiz, and Duygu Senol for their help in test preparations. Any opinions, findings, conclusions or recommendations expressed in this publication are those of the writers, and do not necessarily reflect the views of the sponsoring agency.

References

1. Doebling SW, Farrar CR, Prime MB (1998) A summary review of vibration-based damage identification methods. *Shock Vib Dig* 30(2):99–105
2. Sohn H, Farrar CR, Hemez FM, Shunk DD, Stinemates DW, Nadler BR (2003) A review of structural health monitoring literature: 1996–2001. Los Alamos National Laboratory report, LA-13976-MS, Los Alamos
3. Turkish Earthquake Code (2007) Specifications for structures to be built in disaster areas. Ministry of Public Works and Settlement, Ankara
4. APS 113 Electro-Seis Data Sheet (2014) APS 113 Electro-Seis long stroke shaker with linear ball bearings, Product Manual
5. Van Overschee P, De Moor BL (1996) Subspace identification for linear systems: theory, implementation, applications, vol 3. Kluwer academic publishers, Dordrecht
6. James GH III, Carne TG, Lauffer JP (1993) The natural excitation technique (NExT) for modal parameter extraction from operating wind turbines (No. SAND-92-1666). Sandia National Labs, Albuquerque
7. Farrar CR, James GH III (1997) System identification from ambient vibration measurements on a bridge. *J Sound Vib* 205(1):1–18
8. Juang JN, Pappa RS (1985) Eigensystem realization algorithm for modal parameter identification and model reduction. *J Guid Control Dyn* 8(5):620–627
9. Brincker R, Zhang L, Andersen P (2001) Modal identification of output-only systems using frequency domain decomposition. *Smart Mater Struct* 10:441–445
10. Chopra AK (2007) *Dynamics of structures*, 3rd edn. Prentice Hall, Upper Saddle River